Distinct roles for sequential NREM and REM acetylcholine-regulated states during sleep-dependent memory consolidation.

Michael Satchell[1], Alexis Simmons[2], Sara J. Aton[3, *], Michal R. Zochowski[1,4, *]

1. Department of Physics, University of Michigan, Ann Arbor, MI, USA
2. Department of Physics, Baylor University, Waco, TX, USA
3. Department of Molecular, Cellular and Developmental Biology, University of Michigan, Ann Arbor, USA
4. Biophysics Program, University of Michigan, Ann Arbor, USA

*** Corresponding authors:**

Sara J. Aton (saton@umich.edu), Michal R. Zochowski (michalz@umich.edu)

Abstract

Across vertebrate species, sleep consists of repeating cycles of NREM followed by REM. However, the respective functions of NREM and REM states, as well as their stereotypic cycling pattern, are not well understood. Here, using a simplified biophysical network model, we show that NREM and REM sleep can play differential and critical roles in memory consolidation primarily regulated, based on state-specific changes in cholinergic signaling. Within this network, decreasing and increasing muscarinic acetylcholine (ACh) signaling during bouts of NREM and REM, respectively, differentially alter neuronal excitability and excitatory/inhibitory (E/I) balance. Learning was modeled in the network as increased firing in a subpopulation of excitatory neurons in the network (engram neurons) during a high-ACh wake-like stated. During subsequent NREM, ACh-regulated current (m-current) causes deactivation of inhibitory neurons, leading to network-wide disinhibition and bursts of synchronized activity led by firing in engram neurons. Together, these features strengthen connections from the original engram neurons to less-active excitatory network neurons, which become incorporated into the memory engram. In contrast, when m-current is blocked during subsequent REM, an increase in network inhibition suppresses firing in all but the most-active excitatory neurons, leading to competitive elimination of newly-recruited neurons from the memory trace. We find that an iterative sequence of state-specific activations during NREM/REM cycling is essential for memory storage in the network, serving a critical role during simultaneous consolidation of multiple memories. When sleep cycles were reversed (i.e., REM followed by NREM), or one longer cycle was substituted for multiple shorter cycles, neither of two memories is successfully consolidated. Together these results provide a mechanistic, testable hypothesis for the respective roles of both NREM and REM sleep, and their universal timing, in memory consolidation.

Introduction

In vertebrate species, sequential cycling from wake to non-rapid eye movement (NREM) sleep to REM sleep is a universal pattern (1). The evolutionary origins of physiologically-distinct NREM and REM states are a matter of speculation (2). However, available data suggest that both are essential for brain functions, including long-term memory consolidation and learning-associated synaptic plasticity (3-6). The two states have dramatically different features – including characteristic neuronal firing patterns and rate changes, network oscillations, and neuromodulation (3-5, 7-12) – suggesting NREM and REM likely have distinct effects on brain circuits during memory storage. Recent studies have identified molecular (13, 14) and electrophysiological (15-25) changes in neural circuits during post-learning NREM and REM sleep. A physiological variable which diverges widely between wake, NREM sleep, and REM sleep is the level of acetylcholine (ACh) release in the forebrain (26). ACh regulates neural excitability, and is essential for brain processes ranging from sleep-wake regulation to sensory detection (27-30). Cholinergic projections are found throughout the forebrain, midbrain and brainstem (31).

In the hippocampus, cholinergic inputs originating in the medial septum (MS)(32)(33) provide direct input to both principal neurons and interneurons (34). The septo-hippocampal projection is a critical regulator of hippocampal function, regulating theta oscillations vital in memory acquisition and storage (35). ACh acts through nicotinic and muscarinic receptors (36, 37). In the hippocampus, the most abundant nicotinic receptor subtypes are $\alpha 7$ and $\alpha 4 \beta 2$ receptors, expressed by pyramidal neurons and GABAergic interneurons (37-40). ACh acts on five subtypes of muscarinic receptors, M1 through M5 (41). M1 muscarinic receptors, expressed on neuronal dendrites or somas, are the most abundant subtype in the hippocampus (42, 43). These receptors regulate the excitability of hippocampal neurons (44, 45) via coupling to slow non-inactivating potassium channels. Regulation of these channels' corresponding ionic current (m-current), blocked when ACh is high, leads to a switch between Type 2 excitability (when concentration ACh is low) and Type 1 excitability (when concentration Ach is high) (46-49). Shifts from Type 1 to Type 2 excitability cause dramatic changes in firing frequency responses to injected current (i.e., f-I curve or gain function) (49). The f-I curve of Type 1 neurons is continuous and has a relatively large firing frequency response to incremental changes in excitatory current (49). Type 2 neurons have a discontinuous frequency increase from quiescence and exhibit relatively small frequency responses to changes in excitatory current (49). A concurrent change at the switch between Type 1 and Type 2 dynamics is a differential response of spike timing (i.e. an advance or delay in

spiking) in response to weak excitatory input – the so-called phase response curve (PRC) (46); A Type 1 PRC is uniformly positive, meaning that excitatory synaptic inputs always advance the timing of the next spike. Type 2 dynamics are characterized by a biphasic PRC, with advances or delays possible (46, 49). The biphasic nature of the Type 2 PRCs mediates spike synchrony among neurons in a network (49, 50). Thus, Ach modulation at M1 receptors can dramatically change neurons' frequency responses to excitatory input, as well as their capacity to synchronize their firing to one another.

ACh may also modulate the relative activity levels of interneurons vs. principal neurons, to alter excitatory-inhibitory balance in brain networks (51, 52). In the hippocampus, ACh has the ability to selectively activate somatostatin-expressing (SST+) interneurons (53-55), which can affect the encoding, storage, and recall of memories. Inhibitory gating of activity in the DG network by SST+ interneurons in the hours following learning constrains hippocampal memory consolidation (56). Chemogenetic suppression of medial septal ACh projections to hippocampus after single-trial fear conditioning improves sleep-dependent fear memory consolidation and increases DG granule cell activity. Conversely, chemogenetic activation of ACh inputs suppresses DG granule cell activity and impairs memory consolidation (56). These results are consistent with prior research indicating that suppression of cholinergic signaling after learning benefits sleep-dependent, hippocampally-mediated memory consolidation in human subjects (57, 58).

Together, these findings suggest that NREM-associated suppression of ACh input to hippocampus is an essential feature for sleep-dependent memory consolidation. However, there are accumulating data suggesting that REM – a high-ACh brain state - also plays an important role in consolidation of hippocampus-dependent memories (59-62). Yet it remains unclear whether NREM and REM play overlapping, distinct, or complementary roles in the storage of information in neural networks. How the bidirectional changes in cholinergic signaling during these two states affect the dynamics and function of hippocampus is largely unknown.

Here, using *in silico* models, we investigate ACh-regulated mechanisms underlying differential NREM- and REM-specific effects on memory storage in neural networks. We show that disinhibition and excitability changes in principal cells, mediated by activation of m-current in response to reduced ACh signaling during NREM, increases recruitment of new neurons into newly-encoded memories' engrams. In contrast, increased activation of inhibitory interneurons when m-current is blocked by ACh signaling during REM leads to competitive and selective pruning of neural representations associated with given memories. This REM-dependent mechanism is specifically important when multiple memories are to be consolidated

simultaneously, as it naturally reduces overlap between different memory representations following a period of NREM. Repeated iterations of the NREM→REM cycle (such as those occurring across a night of sleep) leads to progressive expansion and segregation of memory traces in the network. Critically, reversal of the NREM→REM sequence (i.e., REM→NREM) led to failure of memory trace expansion. Together these data suggest that NREM and REM could play distinct and complementary roles in memory storage in the hippocampal network, and that the NREM→REM state sequence, which is so universal across various animal species, is an essential feature for memory consolidation.

Results

ACh-regulated neural network state transitions and recruitment of neuronal populations

We used a reduced network to model ACh-dependent effects of NREM and REM sleep on previously-encoded memories. Based on experimental data (63), we constructed a reduced network composed of three cell populations. Within the model, initial memory traces (or "backbones") are formed with a limited number of engram cells (i.e., excitatory neurons that are highly active). This highly-active backbone population comprises the first of the three cell populations. The second population is composed of non-backbone excitatory neurons that are less excitable (LE) due to weaker excitatory connections and increased input from inhibitory interneurons. The excitatory synapses impinging on these neurons (both the connections emanating from excitatory backbone cells and reciprocal connections within this population) undergo spike timing dependent synaptic plasticity (STDP). The two excitatory networks have sparse (~10%), largely random connectivity, with fast AMPA receptor kinetics (see **Methods**). Finally, the network also contains an interneuron population, which inhibits both the backbone neurons and the LE population. This interneuron population is numerically smaller, but with a high connectivity density (50%). Consistent with available data (CITE), these interneurons differentially target the backbone and LE populations, providing a higher level of inhibition to LE neurons via both fast $GABA_A$ receptor signaling and slow receptor kinetics (see **Methods**). All three populations exhibit state-dependent changes in ACh signaling, modeled as a change in m-current conductance. Low concentrations of ACh, present during NREM sleep, are modeled as high m-current conductance ($g_{Ks} = 1.5\,\frac{\mathrm{mS}}{\mathrm{cm}^2}$), while high ACh concentrations, present during REM sleep, are modeled as low m-current conductance ($g_{Ks} = 0\,\frac{\mathrm{mS}}{\mathrm{cm}^2}$).

We first investigated population activation patterns as a function of m-current conductance (**Fig. 1**) for a network with a single encoded memory (i.e., backbone population; **Fig. 1A**). Mean firing frequency changes for neurons within each population (i.e., backbone neurons, LE layer cells and inhibitory interneurons) was measure as g_{Ks} was varied from 0 to 1.5$\frac{\mathrm{mS}}{\mathrm{cm}^2}$.

High conductance of m-current during NREM (representing low ACh levels) on an individual cell level flattens the i-f curve lowering the firing frequency of the affected neurons for a given current injection (49, 64). Thus, during NREM, when g_{Ks} is high, the inhibitory interneurons are less active disinhibiting the LE population. Therefore, the LE layer neurons are more easily recruited into synchronous bursts of activity driven by backbone cells (Fig. 1B, top). These synchronous bursts across the backbone population are mediated through type 2 neural excitability and are associated with biphasic PRCs (46, 50, 65-67). The firing of the backbone cells, on the other hand, is attenuated due to flattened i-f curve, as the disinhibition affects them less due to stronger intra connectivity and weaker overall inhibitory inputs. The kinetics of the type 2 excitability leads to formation of theta oscillation in the backbone population, while a new oscillatory band emerges at ~6Hz (Fig. 1C top-left), driven by the recruitment dynamics of the LE layer (Fig. 1C top-right). Subsequently, during NREM (high g_{Ks}) we observe a heterogeneous response of the cell populations in the network. The firing frequency of both inhibitory interneurons and backbone neurons (Fig. 1D; green bar, dark blue and red lines) is attenuated. At the same time, due to strong coupling from the inhibitory cell layer to the LE layer cells, lowering activation of the inhibitory interneurons results in disinhibition of LE layer neurons and an increase in their firing rate (Fig. 1D; green bar, teal line).

When ACh signaling is high ($g_{Ks} = 0$; e.g., during REM) both backbone and inhibitory interneurons exhibit highly synchronous periodic activation at theta frequency (**Fig. 1B**), which is driven by slow interneuron-driven inhibitory current targeting the backbone neurons. Here, this mechanism is similar to that underlying pyramidal interneuron gamma (PING) (68, 69), but acts at a lower frequency determined by slow inhibitory receptor kinetics. The activation of excitatory backbone neurons generates a burst of firing among the interneurons, which in turn synchronously inhibits excitatory population until the slow inhibitory postsynaptic current (IPSC) decays, allows the backbone cells to subsequently fire again. Since the LE neurons are more strongly inhibited by the inhibitory cells, they do not activate during that process, and their firing pattern is driven by random noise input (see methods). Hence, the population dynamics results

in strong spectral power in the theta band for the whole network (Fig. 1C bottom-left) driven primarily by the activation of backbone cells and inhibitory interneurons (Fig. 1C; bottom-right). Thus, during REM, we observe strong activation of backbone layer and inhibitory interneurons (Fig. 1D; red bar, dark blue and red lines), but attenuation of LE layer activity (Fig. 1D; red bar, teal line).

We next investigated how REM and NREM differentially recruits LE cell populations receiving two levels of input from backbone cells (Fig. 2). Here, we divided the LE layer population into two groups where one receives only weak coupling from backbone cells, while the coupling of the other group with backbone cells is strengthened by a positive multiplier $M_{ij} \in [1.0\,, 6.0]$, Fig. 2A. We monitor population response of the cells in LE layer as a function of the multiplier (M_{ij}) magnitude during NREM and REM-like states.

During NREM, the LE population is disinhibited due to decreased spiking activity of inhibitory cell layer (Fig. 2B; top, red line) allowing for both LE layer groups (i.e., with and without multiplier) to spike. This in turn allows for population burst of activity synchronizing both backbone cell layer and whole LE layer, with subsequent recruitment of both LE populations (Fig. 2C, top). Subsequently, with STDP present this leads to structural recruitment of both LE populations into the engram.

At the same time, during REM, when m-current is blocked, strong inhibition from the interneuron layer (Fig. 2B bottom, red line) allows for activation of only LE layer cells with strong input from backbone layer (i.e., high M_{ij}), while keeping the other LE population inactive (Fig. 2B, bottom, teal line). The activated LE cells are triggered by a strong burst from backbone cells and synchronize with them forming a strong population burst (Fig 2C, bottom). This in turn triggers STDP-mediated strengthening of connections between backbone cells and the activated LE layer population, while the connections to the other LE group are attenuated.

Differential Recruitment of LE cells into multiple memories during NREM and REM sleep

Having characterized network activation and recruitment patterns as a function of m-current activation representing NREM or REM sleep states, we turn to investigate how the NREM and subsequent REM-like states affect memory consolidation (i.e., recruitment in LE cell layer) when multiple (two) memories (Fig. 3A) are being reactivated (Fig. 3B-G; left column). We also test the effects of the reverse sequence, when the REM-like sleep state precedes the NREM-like state (Fig. 3BB-GG; right column). The reactivation of the two memories is represented via activation

of two independent (i.e. no reciprocal cross-connections) backbone groups (blue and green, Fig 3B, neuron IDs 100 and above).

We monitor effects of this sleep dependent memory consolidation during test epochs that happen before sleep consolidation (control), and then after each sleep state (Fig. 3B). During the test phases, which loosely represent a waking state recall, the m-current is low (i.e., ACh release is high), there is no synaptic plasticity and the backbone cells belonging to one of the two memories are activated continually.

The NREM and REM - like sleep states are defined through their m-current conductance (i.e., m-current is high for NREM and low for REM sleep) and presence of synaptic spike timing dependent plasticity (STDP). This plasticity takes place between the backbone and LE layer, and within the LE layer population. Here, instead of spontaneous reactivation of the memories we drive reactivation of the backbone cells via periodic current injection at theta frequency, and monitor subsequent activation and recruitment of the LE layer neurons into the memory engram. The duration of the current pulse, as well as temporal separation of the reactivated memories were subject to parameter scans to ensure generality of the presented results (Fig. 1S and Fig. 2S; supplemental material).

Since the connections from each backbone are assigned randomly to the LE layer neurons, the number of connections every neuron receives from either backbone varies. For visualization purposes we divided the LE layer population into four quartiles (Fig. 3B and BB): 1) preferential attachment to memory 1 – 50% of LE neurons receiving most synaptic inputs from backbone representing memory 1 and receiving least synaptic inputs from memory 2; (cells denoted as blue in the LE layer – gray background), 2) preferential attachment to memory 2 - 50% of LE neurons receiving most synaptic inputs from backbone representing memory 2 and bottom 50% of LE neurons receiving least synaptic inputs from memory 1 (cells denoted as green in the LE layer – gray background), 3) bottom 50% of LE neurons that receive least connections from either of the memories (neurons denoted as pink in the LE layer) and, 4) top 50% of the LE neurons that receive most connections from both of the memories (neurons denoted as violet in the LE layer).

In addition, the pink and violet groups are representing inactivated control populations as their constant current input is set so that the cells fire only sparsely and randomly, driven by noise rather than synaptic inputs.

When presented NREM -> REM sequences (Fig. 3A), we observe that during pre-sleep testing phase the blue and green LE groups fire only sparsely as the corresponding backbones are

activated. During the following NREM sleep phase when the LE cells experience disinhibition, both the blue and green LE groups are activated, largely independent of the activated backbone memory. That leads, via STDP, to indiscriminate potentiation of the connections between both backbone and LE layer. Subsequently during the testing phase, we see increased and overlapping activation of the LE groups, only partially modulated by the identity of the activated backbones.

During REM, however, when inhibition to the LE layer is significantly stronger, neurons in the LE layer fire more sparsely and lock more discriminately to the backbone they have preferential attachment to (i.e., green LE cells lock to the green backbone, and blue LE cells to the blue backbone). This results, via STDP, in weakening of the cross-connections between nonmatching backbone and LE populations. During the subsequent test phase, one observes larger differentiation of between the activated LE populations as the activated backbones are being switched – recruited LE cells form to a large degree non-overlapping populations, separating memory 1 and memory 2 engrams.

However, when the order of sleep phases is reversed (namely REM precedes NREM) we observe diametrically different memory consolidation dynamics (Fig. 3BB). Now, the increased inhibition during REM effectively prohibits activation and STDP-mediated recruitment of the LE layer neurons. This results in depotentiation of the backbone – LE layer connections making subsequent recruitment in the following NREM phase impossible, as the synaptic inputs are now too week to drive bursting throughout the LE layer. The end result is a lack of engram enlargement.

To assess quantitatively effects of memory consolidation through recruitment of LE cells to memory representation we characterized changes of four observables during the three test epochs (i.e., pre-sleep, post NREM (or REM), post NREM+REM (or REM+NREM): 1) changes in firing frequency of the respective groups in LE layer (Fig. 3C and CC); 2) changes in synaptic connectivity between memory backbones and specific neuronal groups in LE layer (Fig. 3D and DD), and 3) changes in patterns of functional connectivity between the LE neurons (Fig. 3E-G and EE-GG).

The firing frequency of neurons in the LE layer that are preferentially coupled to memory backbones dramatically increases during the post-NREM testing phase as compared to pre-sleep control. The activation of the two LE groups is biased towards backbones that they share the highest number of connections with, but there is a significant overlap between the two groups.

After subsequent REM the difference in activation between the two LE groups increases showing larger separation between the two recruited cell populations (Fig. 3C). Thus, the sleep memory consolidation results in recruitment of a significant number of LE layer neurons, keeping at the same time significant activity separation between the neurons.

In contrast, when the sleep phases are reversed (i.e., REM precedes NREM) the activation of neurons in the LE layer collapses to baseline during REM and only minimally recovers after subsequent NREM (Fig.3CC) - sleep lacks significant recruitment of new cells into the memory engram.

We monitored changes of total connection strength between memory 1 / memory 2 backbones and the neuronal subgroups in LE layer. Figure 3D and DD (top) depict sample distributions of total connection strengths from memory1 (x-axis) / memory 2 (y axis) backbones to all neuronal subgroups of LE layer for a single simulation run during pre-sleep, post-NREM and post REM testing epochs. The green and blue groups within LE layer are by their definition predisposed to have stronger connection with memory1/memory 2, respectively. The pink and violet groups lie on the diagonal, indicating similar total connection strength to both memory backbones. After NREM sleep consolidation both green and blue groups in LE layer strengthen their connections along both axes indicating significant crosstalk between memory backbones and LE layer groups. At the same time, due to sparse random activation, the pink and violet groups are synaptically decoupled from the backbones. The mean change of total connection strength between pre-sleep and NREM test epochs (averaged over five simulation runs) is depicted on bottom of Fig 3D and DD. The colored vectors correspond to the shift of mean total connection weight for the corresponding groups between pre-sleep test and post NREM test (Fig. 3D; left bottom panel).

After subsequent REM sleep consolidation, separation of synaptic targets in the LE layer takes place: the blue group in the LE layer now receives predominantly input from the memory 1 backbone, whereas the green group receives the same from the memory 2 backbone. This mean change can be again visualized by the vectors denoting change in total connection strength between post NREM and post NREM + REM test phases (Fig. 3D, bottom center plot). Ultimately, the NREM+REM sequence results in separate populations of LE layer neurons undergoing strong potentiation from the two memory in an orthogonal manner (Fig. 3D, bottom right plot). When the order of the NREM/REM sequence is reversed the connectivity between the backbones and LE layer withers (Fig. 3DD), effectively disconnecting the LE layer neurons from the backbone.

Next, we analyzed emergence of patterns of functional connectivity within the LE layer neurons. We used a functional connectivity algorithm (FCA) that we had developed earlier (see methods for brief description) and monitor emergence of pairwise, temporal coactivation patterns between the active LE layer neurons when memory 1 backbone and memory 2 backbones are activated separately. The robustness of the emerging synchrony is established via comparison to randomized spike trains and the results are reported as a z-score (Fig. 3E, one sample run). The LE cells are ordered to represent the four groups as described above and shown on the raster plot, with the violet group having the lowest neuron IDs and the green group having the highest ones.

We compared functional connectivity patterns for pre-sleep, post NREM and post NREM+REM sequence testing periods. No significant functional connectivity between cell pairs was observed during pre-sleep test period. Strong synchrony was however observed post NREM, with neurons belonging to both green and blue groups showing intragroup and intergroup synchrony. The neurons belonging to both pink and violet group did not exhibit any significant intergroup or intragroup functional connectivity.

After the NREM+REM sequence the LE layer population exhibiting synchronous firing was pruned, with predominantly intra group connectivity present. This indicates that while during NREM, LE layer neurons form functional clusters that are being recruited into memory representations, REM prunes this population separating the recruited representations into orthogonal clusters at the same time. This is further quantified by computing the overlap between the LE layer populations exhibiting functional connectivity when backbones representing memory 1 or memory 2 are separately activated, and measured during the three test phases (Fig. 3F). This overlap is zero during pre-sleep test phase as the neurons fire randomly. It increases significantly during NREM sleep indicating overlap between memory 1 and memory 2 activated groups in LE layer. After the NREM+REM sequence the overlap between the two populations decreases significantly showing separation between the two activated populations.

Again, when the sleep sequence is reversed (REM +NREM) the functional connectivity clusters do not form (Fig. 3EE) and the population overlap remains zero (Fig 3FF), indicating lack of recruitment of LE layer neurons into the memory engrams.

Finally, we investigated how functional connectivity within the LE layer evolved on a population level during different sleep phases. Namely, we measured the distribution of pairwise changes in the functional connectivity between all neuronal pairs in the LE layer (Fig. 3G). We observed that

during NREM sleep most of the connections undergo strengthening as the distribution is strongly skewed towards positive values (Fig. 3G, left panels).

In contrast, when the post NREM pairs are compared with their post REM values, one observes that the tendency of connections is to weaken, with a small fraction of connections that strengthen significantly even compared to NREM (Fig. 3G center panels). This indicates that while pruning and loss of functional connectivity is the predominant effect of REM, some functional connections get stronger.

As a last step we compared changes in the functional connectivity between the pre-learning test phase and the post NREM+REM test phase. We observe that while most connections do not see significant change in their strength, there is a fraction of connections that strengthen. These connections belong to the cells that are getting selectively recruited into either of the engrams (Fig. 3E).

At the same time, when the sleep sequence is reversed (REM+NREM) we do not observe significant changes in functional connectivity on population level (Fig 3EE - GG) as no recruitment of LE layer neurons takes place.

Significance of multiple sleep sequences

Sleep, across species, is fragmented into relatively short sequences of NREM and subsequent REM, or as is in case in humans, these sequences follow each other throughout a longer sleeping period. The question we investigate here is why it might be benefitial to have multiple cycles of NREM and REM sleep rather than cumulate all the NREM and REM sleep periods together. To that effect, we ran two sets of simulations: in the first set we divided the sleep period into four cycles in which NREM precedes NREM, with each sleep cycle followed by a testing period (Fig. 4A, B). In the second set of simulations, we ran a single cycle of the NREM+REM sequence, with the duration of both NREM and REM matching the total length of the sleep states from the first simulation (Fig. 4C, D).

We monitored activation of LE layer neurons during every test period (Fig. 4B). We observed that systematically after every cycle of sleep, the green and blue LE group activate preferentially with their respective memory backbone, maintaining minimal cross activation. In the second set of simulations, when there is single sleep cycle having duration equal to the combined four sleep cycles, we observe significant co-activation of the LE layer cells during test periods (Fig. 4C, D). We quantified this effect by defining parameters that we refer to as “activation” and “separation”

(Fig. 4C; see methods). Activation (black line) averages the mean firing frequency of the green and blue LE layer groups when their corresponding backbone population is activated during each test phase. Separation (red line) refers to normalized difference in mean firing frequency between the green and blue LE layer groups during their respective testing phases. We observe that both activation and separation increase steadily as a function of the number sleep cycles. The activation for non-participating LE layer groups (denoted as before by pink and violet) does not change throughout the sleep cycles (green line).

When, however, the values of activation and separation are computed for a single sleep cycle consisting of only one NREM followed by one REM period, the results are critically different. The two LE layer groups activate significantly more than during cycling sleep, but their separation dips in comparison, meaning that while the two groups are recruited into the memory more that during cycling sleep, the crosstalk between the recruited populations is much larger. This is due to the fact that during the session of extended NREM in single-cycle sleep, connections to and between the green and blue LE neurons get highly potentiated. The crosstalk connections are then too strong and cause activation of both groups consistently and simultaneously during REM, preventing sufficient pruning and orthogonalization.

Discussion

While it is well known that across vertebrates sleep stereotypically consists of repeating cycles of NREM followed by REM sleep, the roles of NREM and REM play in memory consolidation as well as the function of this cycling are not known. The putative role of sleep varies widely from active an process of memory consolidation (70) to homeostatic regulation of network activity and connectivity (71). Here we show in a simplified biophysical model, that both NREM and REM sleep may play differential and critical roles in sleep dependent memory consolidation, and that their specific function may be mediated via muscarinic pathway response to changing concentrations of ACh.

The network consists of two populations of excitatory pyramidal cells: the backbone cells that form memory representations during active waking, and the less excitable (LE) excitatory cell layer from which additional neurons are recruited into memory representation during sleep. These two populations exhibit different activation properties, as the backbone cell activate stably during both NREM and REM sleep, while the LE neurons undergo changes in their firing pattern during recruitment into memory engrams. Such heterogenous properties of engram cells match those observed experimentally, where sequences of place-cell firing in a novel environment are formed

from a combination of the contributions of a rigid, predominantly fast-firing subset of pyramidal neurons with low spatial specificity and limited change across sleep-experience, and a slow-firing plastic subset (63).

We show that changing ACh level during NREM and REM sleep directly modulates neuronal excitability via muscarinic pathway, and that this in turn affects E/I balance in the network. During NREM, m-current mediated deactivation of inhibitory cells causes disinhibition that allows for recruitment of initially less active excitatory neurons into the memory engram. The recruitment itself happens through synchronized bursts of activity driven by the backbone cells that are penetrating into the LE layer (Fig. 1 and 2). In contrast, during REM, when m-current is blocked increased inhibition blocks activation of LE layer neurons (Fig. 1), allowing only for selective activation and competitive pruning of newly formed memory representations (Fig. 2). We further show that this sequence of activations during NREM/REM cycling plays critical role when consolidating multiple memories (Fig. 3), as it allows for engram expansion while keeping the representations of consolidated memories separated. We also show why this stereotypic order of NREM preceding REM is crucial for the success of sleep memory consolidation (Fig. 3) and hypothesize that memory consolidation maybe an iterative process necessitating in repeated cycling of NREM/REM to achieve optimal consolidation and separation of memory representations (Fig. 4).

In terms of network-wide dynamics we observed that during NREM (Fig 1D; low ACh, high g_{Ks}) the disinhibition, mediated by reduced excitability and hence activity of inhibitory interneurons, will cause overall increase in firing frequency and number of recruited neurons in LE layer, while, conversely, REM (Fig 1D; high ACh, low g_{Ks}) will be characterized by rapid decrease in LE population firing frequency and pruning of the neural representations. Similar results were observed experimentally, as Grosmark et al. found that, within NREM episodes, overall firing rates gradually increased. The rate increase within non-REM episodes was offset by a decrease of spiking frequency within the interleaved REM episodes (72).

Here, the mechanism underlying differential roles of NREM and REM during memory consolidation hinges on the role inhibitory interneurons play in sculpturing memory representations (Fig. 2), and ACh mediated regulation of their activity during NREM/REM sleep. It is generally believed that inhibition is critical for memory functions (52) and shapes the organization of hippocampal representations (73). Specifically, similarly to our model, recurrent, feedback inhibition is thought to promote competition amongst pyramidal cells, as it was shown that in vivo reliable spiking of local interneurons is observed after spontaneous pyramidal

firing(74), or after experimentally driven activation of one to several pyramidal cells (75-77). On the other side, optogenetic silencing of robustly coactivating neuronal sub-populations, disinhibits other neurons, which is reflected as an increase in the amount of c-fos in neurons that do not express the silencing opsin (78, 79). Further, experimental results from both humans and animals show that neural inhibition protects memories from interference to permit continual learning (80).

Within both the hippocampus and neocortex, broad subclasses of inhibitory interneurons have been identified based on biomarker expression: those that express parvalbumin (PV+), those that express somatostatin (SST+), those that express vasoactive intestinal peptide (VIP+), and those that express cholecystokinin (CCK+). It has been shown that these populations play differential roles in memory consolidation and sculpting memory representations (52).

Somatostatin interneurons, that next to PV+ comprise the second-largest population of forebrain GABAergic neurons (81, 82), were shown to play critical role in memory formation during wake and sleep. Optogenetic activation of SST+ interneurons in CA1 is sufficient to disrupt spontaneous sharp wave-ripple oscillations (83). Further, chemogenetic inhibition of SST+ interneurons in the DG during contextual fear conditioning (CFC) improves its recall 24 h or even a full week later (79). Similarly, in Dentate Gyrus, granule cell activation during remote recall - mice that are SST+ interneuron-inhibited or -activated during encoding have larger and smaller DG granule cell populations, respectively, activated during recall.

Behaviorally, in terms of memory separation, a recent study showed that optogenetic inhibition of DG SST+ interneurons during training on either a contextual or object-location discrimination task led to deficits at testing 24 h later, but only if the two scenarios being discriminated were highly similar (84). Further, training-targeted chemogenetic inactivation of DG SST+ interneurons increased the activation of surrounding DG granule cells during background conditioning, and selectively increased freezing responses to context re-exposure 24 h after background conditioning (53). These studies suggest that similarly to inhibitory cells in our model, that SST+ interneuron activation during memory encoding effectively gates the activation of surrounding excitatory neurons.

In terms of SST+ neurons role in memory consolidation, a recent study assessed the effects of chemogenetically activating or inhibiting DG SST+ interneurons over the hours following CFC (56). They found that these manipulations were sufficient to disrupt or enhance CFM consolidation, as evidenced by decreased or increased contextual freezing responses, respectively, 24 h after training. Furthermore, it was found that chemogenetic activation or

inhibition during the consolidation phase reduced or increased cFos expression among DG granule cells, respectively. These data suggest that inhibitory gating of activity in the DG network (and the engram neuron population) by SST+ interneurons in the hours following learning constrains hippocampal memory consolidation (56).

Recent evidence suggests that acetylcholine has the ability to selectively activate SST+ interneurons in the hippocampus (53, 54); this selective sensitivity is mediated by both nicotinic and muscarinic receptors expressed preferentially on the neurons (55, 85). Acetylcholine release in the hippocampus by medial septal inputs is known to be higher during wake vs. NREM sleep (with release increasing again during REM sleep) (86, 87). Aton lab tested whether gating of the hippocampal network, and CFM consolidation, are affected by manipulations of hippocampal cholinergic input. They that, similarly to the results of chemogenetic manipulation of SST+ interneuron activity, chemogenetic suppression of medial septal cholinergic neurons after CFC resulted in greater DG network activity. On the other hand, Chemogenetic activation of cholinergic inputs resulted in suppression of DG network activity (56).

Thus, our results form a congruent picture of differential roles that REM and REM play in sleep dependent memory consolidation. However, there are clear limitations to this study: we only consider muscarinic effects of ACh dependent sleep modulation. Nicotinic ACh pathway and other neuromodulator systems may also play an important role in regulation of network dynamics remodeling during sleep (88, 89). Further, we do not include sleep dependent changes in input to the network (e.g. thalamic role in formation of NREM spindles (90)**.**

Taken together we provide a testable hypothesis of ACh mediated differential roles that NREM and REM sleep play in sleep dependent memory consolidation. We show the importance of the stereotypic order of this process (i.e, NREM preceding REM) and its iterative (cycling) nature. We believe that the role of REM based pattern separation will be specifically important for storage of correlated (in terms of time and content) memories.

Methods

Neuron Model

The excitatory and inhibitory neurons were modeled using a conductance-based Hodgkin-Huxley formalism *(65, 91)*. The time-dependent voltage V_i of an individual neuron is given by the master equation:

$$C\frac{dV}{dt} = -g_{Na}m_{\infty}^{3}(V)h(V)(V - V_{Na}) - g_{Kdr}n^{4}(V)(V - V_{K}) - g_{L}(V - V_{L}) - g_{Ks}z(V)(V - V_{K}) + I_{drive} + I_{noise} - I_{syn}$$

with the first four currents from left to right on the RHS representing a fast inward Na^+ current, a delayed rectifier K^+ current, a membrane leak current, and a slow outward (hyperpolarizing) K^+ current representative of muscarinic m_1 receptor activation (m-current). The m-current conductance, g_{Ks}, is a proxy for the state dependent ACh level, with ACh blocking the activation of this current, i.e. during NREM sleep when ACh levels are low, m current is high ($g_{Ks} = 1.5\,\frac{\mathrm{mS}}{\mathrm{cm}^2}$); and conversely, during REM sleep when ACh concentration is high, m-current is blocked ($g_{Ks} \rightarrow 0$). On a cellular level, the presence of m-current via g_{Ks} conductance modulates membrane excitability, with low g_{Ks} (high ACh) yielding Type 1 excitability, whereas high g_{Ks} (low ACh) yielding Type 2 excitability. Type 1 excitability is characterized by arbitrarily low firing frequencies, high frequency gain as a function of constant input, and advance-only phase response to brief stimulation pulse (i.e. phase response curve, PRC). Type 2 excitability has a threshold in firing frequency onset, a shallow frequency gain function, and a biphasic phase response curve *(65)*.

The parameters in the above equation are the same for describing either excitatory pyramidal neurons or inhibitory interneurons and are provided in table 1.

Parameter	Value	Units
C	1	$\frac{\mu\mathrm{F}}{\mathrm{cm}^2}$
g_{Na}	24	$\frac{\mathrm{mS}}{\mathrm{cm}^2}$
g_{Kdr}	3	$\frac{\mathrm{mS}}{\mathrm{cm}^2}$
g_{Ks}	0 – 1.5	$\frac{\mathrm{mS}}{\mathrm{cm}^2}$

$\boldsymbol{g_L}$	0.02	$\frac{\mathrm{mS}}{\mathrm{cm}^2}$
$\boldsymbol{V_{Na}}$	55	mV
$\boldsymbol{V_K}$	-90	mV
$\boldsymbol{V_L}$	-60	mV

The gating variables, i.e., sodium inactivation, $h(V)$, potassium activation, $n(V)$, and m-current activation, $z(V)$, are given by:

$$\frac{dh}{dt} = (h_\infty(V) - h)\frac{1}{\tau_h(V)}$$

$$\frac{dn}{dt} = (n_\infty(V) - n)\frac{1}{\tau_n(V)}$$

$$\frac{dz}{dt} = (z_\infty(V) - z)\frac{1}{75}$$

where $h_\infty(V)$, $n_\infty(V)$, $z_\infty(V)$, $m_\infty(V)$, $\tau_\mathrm{h}(V)$ and $\tau_\mathrm{n}(V)$ are defined as:

$h_\infty(V) = \frac{1}{1+e^{\frac{V+53}{7}}}$,

$n_\infty(V) = \frac{1}{1+e^{\frac{-V-30}{10}}}$,

$z_\infty(V) = \frac{1}{1+e^{\frac{-V-39}{5}}}$,

$m_\infty(V) = \frac{1}{1+e^{\frac{-V-30}{9.5}}}$,

$\tau_h(V) = 0.37 + \frac{2.78}{1+e^{\frac{V+40.5}{6}}}$,

$\tau_n(V) = 0.37 + \frac{1.85}{1+e^{\frac{V+27}{15}}}$,

with the time constants in [*ms]* and voltages in [*mV]*.

The terms I_{drive}, I_{noise}, and I_{syn}, each in $\frac{\mu\mathrm{A}}{\mathrm{cm}^2}$, are inputs to the neuron representing depolarizing constant current, random external input, and synaptic input from other neurons of the modeled circuit, respectively.

The external driving current I_{drive} is a network-controlled parameter used to set the excitability of neurons. For excitatory neurons $I_{drive} = 0.5\,\frac{\mu A}{cm^2}$ unless otherwise specified, and for inhibitory neurons $I_{drive} = -0.1\,\frac{\mu A}{cm^2}$. This difference in activations effectively ensures that inhibitory neurons do not fire autonomously but only in response to excitatory input.

Synaptic connectivity

Once a neuron's membrane voltage exceeds preset threshold (5 mV), a spike is recorded, and the presynaptic cell activates (inhibitory or excitatory) post synaptic current to all its postsynaptic targets. The postsynaptic currents, $I_{syn}^{i}(t)$, received by an (i-th) cell are modeled as a linear combination of fast and slow excitatory and inhibitory currents.

$$I_{syn}^{i}(t) = \sum_{j}^{N_e}\sum_{k} A_{ij}M_{ij}w_{ij}^{E}(V_i - E_{rev}^{E})R^{E}\exp\left(\frac{t-t_{jk}}{\tau_f}\right) + \sum_{l}^{N_i}\sum_{m} A_{il}M_{il}w_{il}^{I}(V_i - E_{rev}^{I})\left(R_f^{I}\exp\left(\frac{t-t_{lm}}{\tau_f}\right) + R_s^{I}\exp\left(\frac{t-t_{lm}}{\tau_s}\right)\right)$$

Where t_{jk} is the timing of k-th spike on j-th neuron; R^E, R_f^I, R_s^I denote relative amplitudes of excitatory, fast inhibitory and slow inhibitory currents, respectively. The $\tau_f = 0.5\,ms$ and $\tau_f = 50\,ms$ are the time costants defining time course of fast and slow post-synaptic currents. $E_{rev}^{E} = 0\,mV$, $E_{rev}^{E} = -75mV$ are the reversal potentials for excitatory and inhibitory currents respectively; M_{ij} denotes synaptic multiplier differentiating synaptic efficacy originating/ targeting different cell populations (see table 2); finally w_{ij}^{I} and w_{ij}^{E} are synaptic weights describing excitatory and inhibitory connectivity strengths between *i*-th and *j*-th neurons, and $A_{ij} =$ Error! Bookmark not defined. denotes terms in the adjacency matrix.

Synapse Type	**Postsynaptic Neuron Type**	
	Excitatory	Inhibitory
R^e	0.15	0.08
R_f^i	0	0.15
R_s^i	0.05	0

$I_{syn}^{i}(t)$is represented in $\frac{\mu A}{cm^2}$.

Synaptic Plasticity

In the simulations that included spike timing plasticity (STDP; Figs. 2-4) the change in synaptic strength between postsynaptic neuron i and presynaptic neuron j was given by

$$\Delta\omega_{ij} = \begin{cases} P_x A_+ \exp -\frac{|\Delta t_{ij}|}{\tau_+} & \Delta t_{ij} > 0 \\ -P_x A_- \exp -\frac{|\Delta t_{ij}|}{\tau_-} & \Delta t_{ij} < 0 \end{cases}$$

where Δt was the difference between the most recent spike time of postsynaptic neuron i and presynaptic neuron j; A_+ and A_- are the maximum rates of change (excluding P_x) with values $A_+ = 0.07$ and $A_- = 0.025$. τ_+ and τ_- are the time constants, $\tau_+ = 14$ ms and $\tau_- = 34$ ms. The overall effect is plasticity that favors potentiation between neurons that spike close in time ($\Delta t < \sim 25$ ms) and favors depotentiation for longer ISIs. This in turn will lead to overall synaptic depotentiation in randomly and sparsely firing network, and conversely - to synaptic potentiation in highly firing network. P_x represents a network wide controlled parameter for changing the rate of plasticity between specific neuron groups. The synaptic weight w_{ij} for each connection is constrained to the interval [0, w_{max}] where $w_{max} = 5$. Plasticity is reserved for connections between excitatory neurons, so connections involving an inhibitory neuron always feature $w_{ij} = 1$.

Plasticity rates vary between some groups of neurons and are controlled by the set of parameters P_x shown below.

P_x		**Postsynaptic**		
		Backbone neurons	LE layer neurons	Inhibitory interneurons
Presynaptic	Backbone neurons	1	1	0
	LE layer neurons	0.3	0.3	0

	Inhibitory interneurons	0	0	0

External random input

External random input in the network, representing input from other external modalities, is modelled by a low-probability excitatory current influx to each neuron. Every millisecond there is a 0.002% chance that a given neuron will receive an $I_{drive} = 80\ \frac{\mu A}{cm^2}$ input with duration of 1 ms. This results in random firing 2 Hz for all neurons in the network.

Network Connectivity

The two-memory network is composed of 160 excitatory pyramidal and 20 inhibitory neurons. The excitatory neurons are sparsely and randomly connected with 10% connectivity (with connections emanating to both other excitatory cells and inhibitory cells). Inhibitory cells neurons are connected at random to 50% of neurons in the network (both excitatory and inhibitory). The relative synaptic efficacy between the three populations (M_{ij}) are described in a table below (table 2)

Excitatory neurons are divided evenly into two groups, initial memory backbone (BB) neurons and less activated (LE) neurons. The backbone neurons represent the initial (one or two) memory traces stored during active waking (not modeled here). These neurons receive less inhibition than LE cells and the synaptic weights between neurons of a single backbone remain fixed. Importantly, there are no connections between backbone neurons belonging to different memories. The LE neurons represent the population of excitatory cells that fire less because of increased inhibition from inhibitory interneurons. All excitatory synaptic inputs targeting this population (both from the BB population and other LE neurons) undergo spike timing dependent plasticity as described above.

M_{ij}		**Postsynaptic**		
		Backbone	LE layer	Inhibitory interneurons
Presynaptic	Backbone	1	1	1
	LE layer	1	1	1

	Inhibitory interneurons	0.5	3.5	1

Two-memory consolidation network

If representations of two memories are stored in the network (as in Fig. 3), the backbone group is divided into disjoint sets of neurons. Those two sets do not share synaptic connectivity, but randomly target the inhibitory and LE cell populations. Since the connections from each backbone are assigned randomly to the LE layer neurons, the number of connections every neuron receives from either backbone varies. We divided the LE layer population into four quartiles: 1) **preferential attachment to memory 1 (cells denoted as blue in the LE layer – gray background)** - top half population of LE neurons receiving most connections from backbone representing memory 1 and bottom half population of neurons receiving least connections from memory 2; 2) **preferential attachment to memory 2 (cells denoted as green in the LE layer – gray background)** - top half population of neurons receiving most connections from backbone representing memory 2 and bottom half population of neurons receiving least connections from memory 1; 3) bottom half population of neurons that receive least connections from either of the memory (neurons denoted as pink in the LE layer), and, 4) top half population of the neurons that receive most connections from either of the memory backbone (neurons denoted as violet in the LE layer).

Activity Analysis:

Measurement of firing frequency response of the LE group

We have calculated average mean spiking rate (Figs. 1 - 4) of the total LE layer population or separately, for subgroups of the LE layer as described above. The mean frequency is calculated as the time-average frequency of each neuron averaged over the whole population in question.

Based on mean spiking activity we have calculated mean activation and separation of LE engram representation for memory 1 and 2. Activation of memory 1 and memory 2 ($A_{1/2}$) is defined as $A_{1/2} = \frac{f_{1/2} - \tilde{f}}{f_{1/2} + \tilde{f}}$, where $f_{1/2}$ is the mean firing frequency of memory1 or memory 2 and $\tilde{f}$ is the mean frequency of the non-activating LE population (groups denoted by pink and purple on the

rasterplot on Fig 3 and 4). It measures activation of the blue and green groups above the background.

On the other hand, separation of memory 1 or memory 2 ($S_{1/2}$) is defined as $S_{1/2} = \frac{|f_1 - f_2|}{f_1 + f_2}$, where f_1 (f_2) is the mean firing frequency of memory1 (memory 2). It measures differential activation of the two LE representations during respective testing phase.

Analysis of backbone-to-LE connectivity

We have calculated the mean synaptic strength received from backbone of memory 1 (x-axis) and that of memory 2 (y-axis) for every subgroup (as defined above) of LE layer neurons, during every test phase. We have then created vectors denoting change in the backbone to every LE connectivity by positioning the vector tail at the onset coordinates and head at the final coordinates. We have constructed these synaptic change vectors between pre-sleep test phase and post NREM sleep test phases (or post-REM sleep phase for the reverse order simulations), post NREM and post-REM testing phases, and between pre-sleep test phase and post-NREM+REM testing phases (or post-REM+NREM testing phase for reverse order).

Functional connectivity within the LE group

To quantify the pairwise functional connectivity between pairs of LE layer neurons (Fig. 3E and EE), a metric based on the average minimal distance (AMD) was used (92). The pairwise AMD between two neurons (*i, j*) was given by the mean difference of the time of each spike, *k* in spike train of the *i*-th neuron, S_i, to the most recent preceding spike in the spike train of *j*-th neuron, S_j. Specifically, the pairwise AMD was given by

$$AMD_{ij} = \frac{1}{N_i} \sum_{k=1}^{N} \Delta t_k^j$$

where N_i was the number of spikes in spike train S_i and Δt_k^j was the temporal distance between *k*-th spike in S_i to the nearest spike in S_j (92).

In order to quantify the magnitude of temporal locking between the pair (i.e., magnitude of functional connectivity), a z-score of the locking was calculated. Briefly, let L be the length of the

interspike interval of the spiketrain S_i. Then the first and second moments (μ_1 and μ_2, respectively) for the spiketrain S_i were given by $\mu_1 = \frac{1}{4T}\sum_L L^2$ and $\mu_2 = \frac{1}{12T}\sum_L L^3$

where T was the total time of the S_i -th spike train (in ms). The moments were used to derive the mean and standard deviation of the minimal distance with respect to S_i where the mean $\mu = \mu_1$, the first moment, and the standard deviation $\sigma = \sqrt{\mu_2 - \mu_1^2}$ (92). Then, the Z-score is given by $Z_{ij} = \frac{AMD_{ij} - \mu_i}{\sigma_i}$.

To establish separation of the two memories (Fig.3F and FF) we calculated dot product of the functional connectivity matrixes when memory 1 and memory 2 are presented during the testing phases. Here data is average over 5 randomly initialized simulations.

To calculate histograms of functional connectivity change (Fig. 3G and GG), we calculated the pairwise z-score difference for every connection pair for the two testing phases in question.

Figure Captions:

Figure 1. M-current regulates differential population of neural activation during NREM-like and REM-like states. A) Diagram of the network: backbone neurons (dark blue), inhibitory interneurons (red), Less Excitable (LE) excitatory layer (teal). B) Sample rasterplot of activation of three populations during NREM (top) and REM (bottom). C) Spectral analysis of observed oscillatory patterning during NREM-like (top) and REM-like (bottom) state. Total network population (left, black line); each cell population separately (colors denoted as above). D) Mean spike frequency of the three network populations as a function of maximal conductance of m-current (g_{Ks}). High m-current conductance observed during NREM sleep (green bar) disinhibits LE population and allows for transmission of population bursts driven by backbone layer; during REM (red bar) backbone neurons are highly active whereas LE cells are shut down by inhibitory interneurons. Results averaged over 5 simulation runs.

Figure 2. REM-like state facilitates differential recruitment of heterogenous LE layer population. A) Diagram of the network: backbone neurons (dark blue), inhibitory interneurons (red), Less Excitable (LE) excitatory layer is divided into two populations: one receiving only basal input from backbone layer (i.e. w/o multiplier; teal) and one receiving variably enhanced input from backbone layer (i.e. w multiplier; violet). B) Average spiking frequency of the four populations as a function of the multiplier (M_{ij}) value during NREM (top) and REM (bottom). C) Sample rasterplot of activation of four populations during NREM (top) and REM (bottom) for multiplier value of $M_{ij} = 5$. NREM-like state allows for indiscriminate recruitment of LE layer cells, whereas REM recruits selectively, only from the population of LE cells having high value of the multiplier M_{ij}.

Figure 3. Differential roles of NREM and REM for consolidation of multiple memories. Stereotypic sleep cycle (i.e., NREM followed by REM; left column) and reversed (i.e., REM followed by NREM; right column). A) diagram of network connectivity. The backbone population consists of separately activated groups coding for memory 1 (blue) and memory 2 (green). B) Sample rasterplot of network activity. The retrieval/activation patterns of LE neurons are tested before the sleep consolidation, after NREM and after NREM+REM. Test phase is defined as high ACh phase with continuous backbone (mem 1 or mem 2) input and no synaptic plasticity. The firing of backbone cells is depicted on the white background (neuron IDs 100-180); firing of LE

layer cells is depicted on gray background (neuron IDs 20-80). LE neurons depicted as blue denote top half population receiving most connections from memory 1 backbone, and bottom half population receiving least connections from memory 2 bacbone; LE neurons depicted as green denote top half population receiving most connections from memory 2 backbone, and bottom half population receiving least connections from memory 1 backbone; LE neurons depicted as pink denote bottom half population receiving least connections from both memory 1 and memory 2 backbones; ; LE neurons depicted as violet denote top half population receiving most connections from both memory 1 and memory 2 backbones. In addition, violet and pink groups receive lower constant current than green and blue rendering them largely inactive throughout dynamics (they fire randomly due to random current received). D) Changes of connectivity between memory backbones (blue - memory 1; green - memory 2) and LE groups (top - sample connectivity maps, bottom - changes of mean connectivity between the test periods, averaged over 5 simulation runs). The X-axis denotes connection weight (top) / mean connection weight (bottom) from memory 1 backbone to LE layer cells; the Y-axis denotes connection weight (top) / mean connection weight (bottom) from memory 2 backbone to LE layer cells. E) Pairwise functional connectivity (measured as synchronous coactivation; see methods) within LE cells; color maps depict statistical significance of coactivation (z-score with respect to bootstrapping) during pre-sleep, post NREM and post NREM+REM tests of a sample run. (F) Overlap between functional connectivity of recruited LE neurons by the two memories, during pre-sleep, post NREM and post NREM+REM tests, averaged over 5 simulation runs. **Significance:** 2 tailed pairwise t-test: Pre-sleep/NREM: $p=0.004$; NREM/MREM+REM: $p=0.033$ (G) Histograms of changes in pairwise functional connectivity after NREM, REM and NREM+REM sleep cycle. NREM sleep indiscriminately recruits LE cells into the engram by primarily strengthening connections from backbone cells to LE population, which results in overlapping functional connectivity patterns within the LE layer. REM prunes these connections, leaving/strengthening only the strongest ones, resulting in separated LE layer engram representations.

Panels BB - GG) same as B – G) for reverse sleep cycle (i.e., REM followed by NREM). Reverse sequence results in loss of connectivity between backbone and LE layer, leading to lack of recruitment of LE layer cells during sleep.

Figure 4. Relative effects of multiple NREM+REM cycles. (A) Sample rasterplot depicting four NREM+REM cycles. Activation test are defined as in Figure 3 and performed after every NREM+REM sequence. (B) Mean spiking activity within LE groups (color scheme is the same as

in Figure 3). (C) Sample rasterplot depicting single NREM+REM cycle of the same combined length as cycles in A. Activation test are defined as in Figure 3 and before and after NREM+REM sequence. (D) Mean spiking activity within LE groups (color scheme is the same as in Figure 3). (E) Changes in activity profiles (activation and separation; see methods) within the LE groups after the sleep cycles are compared to single sleep cycle of cumulatively the same duration (right). Short consecutive sleep cycles result in recruitment of LE layer neurons, but also in separation of the engram representations belonging to different memories; single long sleep cycle results in indiscriminate recruitment of LE cells but lack of separation of the representations belonging to different memories. **Significance:** 2 tailed t-test post fourth sleep cycle/combined sleep length: activation p=0.004; separation p=0.038

Figure 1.

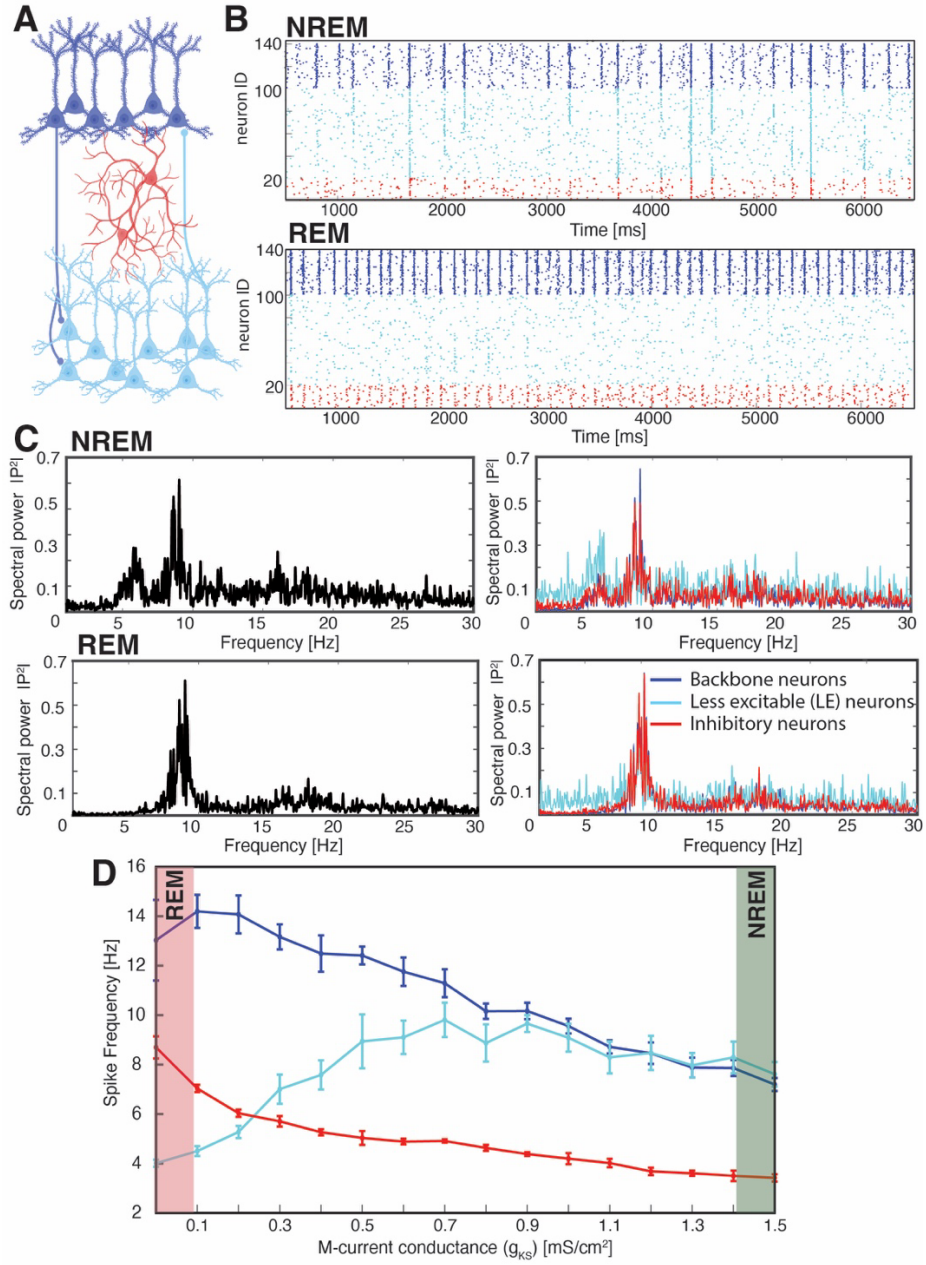
A
B
NREM
REM
neuron ID
Time [ms]
C
Spectral power |P²|
Frequency [Hz]
Backbone neurons
Less excitable (LE) neurons
Inhibitory neurons
D
REM
NREM
Spike Frequency [Hz]
M-current conductance (g_{Ks}) [mS/cm²]

Figure 2.

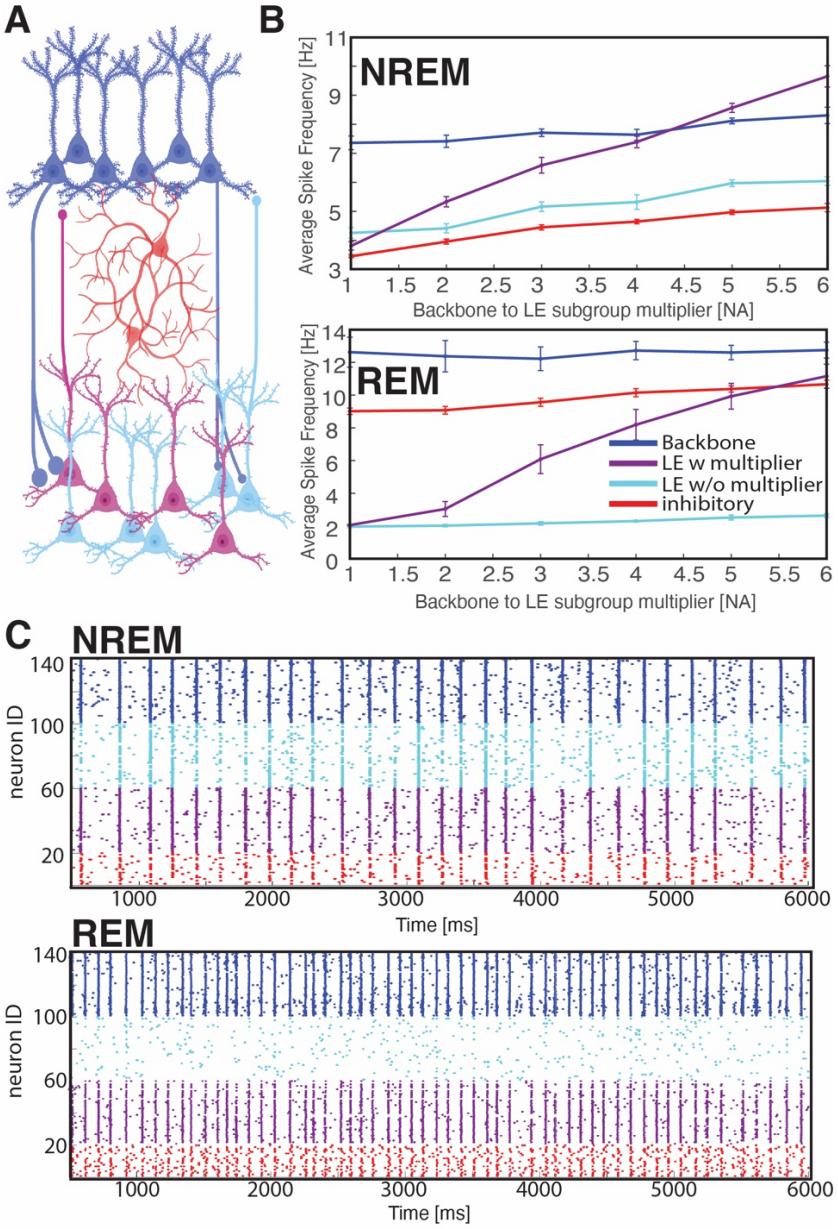
A
B
NREM
Average Spike Frequency [Hz]
Backbone to LE subgroup multiplier [NA]
REM
Backbone
LE w multiplier
LE w/o multiplier
inhibitory
C
NREM
neuron ID
Time [ms]
REM

Figure 3.

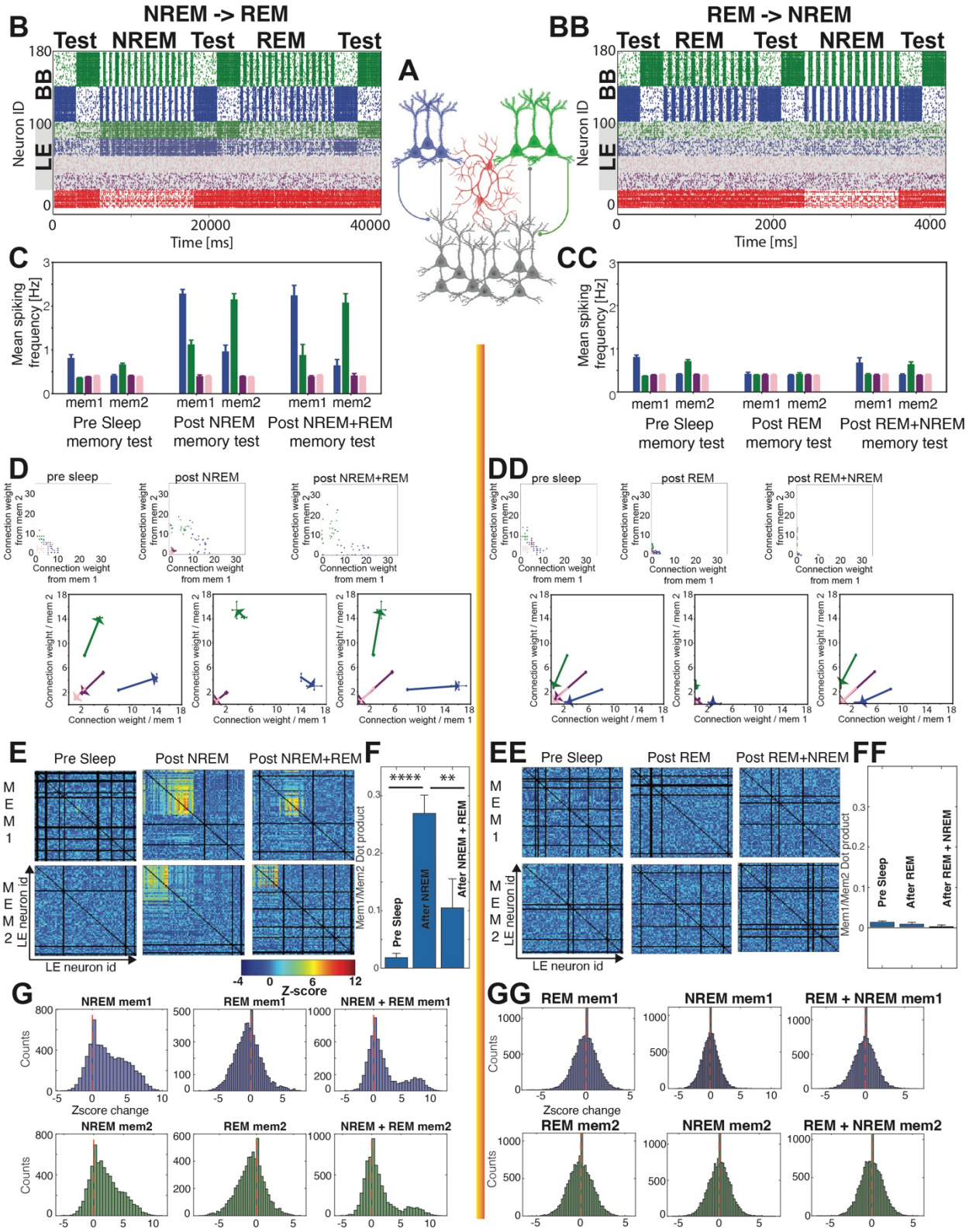
B
NREM -> REM
Test NREM Test REM Test
Neuron ID
BB
LE
Time [ms]
A
BB
REM -> NREM
Test REM Test NREM Test
C
Mean spiking frequency [Hz]
mem1 mem2
Pre Sleep memory test
Post NREM memory test
Post NREM+REM memory test
CC
Pre Sleep memory test
Post REM memory test
Post REM+NREM memory test
D
pre sleep
post NREM
post NREM+REM
Connection weight from mem 2
Connection weight from mem 1
Connection weight / mem 2
Connection weight / mem 1
DD
pre sleep
post REM
post REM+NREM
E
Pre Sleep
Post NREM
Post NREM+REM
MEM1
MEM2
LE neuron id
Z-score
F
Mem1/Mem2 Dot product
Pre Sleep
After NREM
After NREM + REM
EE
Pre Sleep
Post REM
Post REM+NREM
FF
Pre Sleep
After REM
After REM + NREM
G
NREM mem1
REM mem1
NREM + REM mem1
Counts
Zscore change
NREM mem2
REM mem2
NREM + REM mem2
GG
REM mem1
NREM mem1
REM + NREM mem1
REM mem2
NREM mem2
REM + NREM mem2

Figure 4.

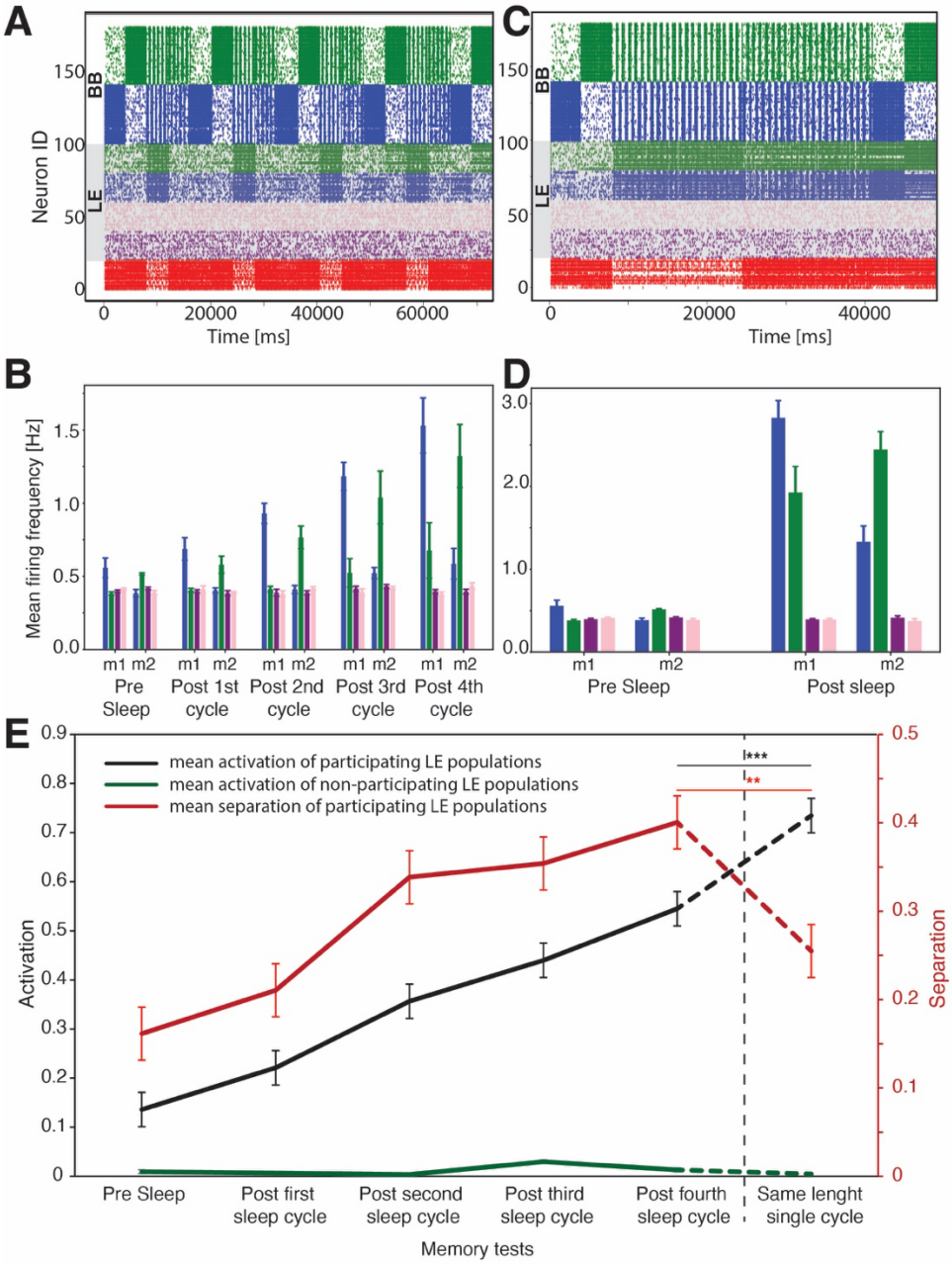
A
C
BB
LE
Neuron ID
Time [ms]
B
D
Mean firing frequency [Hz]
m1 m2
Pre Sleep
Post 1st cycle
Post 2nd cycle
Post 3rd cycle
Post 4th cycle
Post sleep
E
mean activation of participating LE populations
mean activation of non-participating LE populations
mean separation of participating LE populations
Activation
Separation
Pre Sleep
Post first sleep cycle
Post second sleep cycle
Post third sleep cycle
Post fourth sleep cycle
Same lenght single cycle
Memory tests

References

1. R. Yamazaki *et al.*, Evolutionary Origin of Distinct NREM and REM Sleep. *Front Psychol* 10.3389/fpsyg.2020.567618 (2020).
2. C. Puentes-Mestril, J. Roach, N. Niethard, M. Zochowski, S. J. Aton, How rhythms of the sleeping brain tune memory and synaptic plasticity. *Sleep* **42** (2019).
3. C. Puentes-Mestril, J. Roach, N. Niethard, M. Zochowski, S. J. Aton, How rhythms of the sleeping brain tune memory and synaptic plasticity. *Sleep* **42**, pii: zsz095 (2019).
4. C. Puentes-Mestril, S. J. Aton, Linking network activity to synaptic plasticity during sleep: hypotheses and recent data. *Frontiers in Neural Circuits* **11**, doi: 10.3389/fncir.2017.00061 (2017).
5. B. Rasch, J. Born, About sleep's role in memory. *Physiol Rev* **93**, 681-766 (2013).
6. R. Stickgold, J. A. Hobson, R. Fosse, M. Fosse, Sleep, learning and dreams: off-line memory reprocessing. *Science* **294**, 1052-1057 (2001).
7. N. Niethard, H. V. Ngo, I. Ehrlich, J. Born, Cortical Circuit Activity Underlying Sleep Slow Oscillations and Spindles. *Proc Natl Acad Sci U S A* **115**, E9220-9229 (2018).
8. N. Niethard, A. Burgalossi, J. Born, Plasticity during Sleep Is Linked to Specific Regulation of Cortical Circuit Activity. *Front Neural Circuits* **11**, 1-9 (2017).
9. N. Niethard *et al.*, Sleep-Stage-Specific Regulation of Cortical Excitation and Inhibition. *Curr Biol* **26**, 2739-2749 (2016).
10. Y. Zhou *et al.*, REM sleep promotes experience-dependent dendritic spine elimination in the mouse cortex *Nat Communications* **11** (2020).
11. G. Yang *et al.*, Sleep promotes branch-specific formation of dendritic spines after learning. *Science* **344**, 1173-1178 (2014).
12. G. Yang, W. B. Gan, Sleep contributes to dendritic spine formation and elimination in the developing mouse somatosensory cortex. *Dev Neurobiol* **72**, 1391-1398 (2012).
13. S. Ribeiro, V. Goyal, C. V. Mello, C. Pavlides, Brain gene expression during REM sleep depends on prior waking experience. *Learn Mem.* **6**, 500-508 (1999).
14. J. Delorme *et al.*, Sleep loss drives acetylcholine- and somatostatin interneuron-mediated gating of hippocampal activity, to inhibit memory consolidation. *Proc Natl Acad Sci USA* **118** (2021).
15. N. Ognjanovski, D. Maruyama, N. Lashner, M. Zochowski, S. J. Aton, CA1 hippocampal network activity changes during sleep-dependent memory consolidation. *Front Syst Neurosci* **8**, 61 (2014).
16. N. Ognjanovski, C. Broussard, M. Zochowski, S. J. Aton, Hippocampal Network Oscillations Rescue Memory Consolidation Deficits Caused by Sleep Loss. *Cereb. Cortex* **28**, 3711-3723 (2018).
17. N. Ognjanovski *et al.*, Parvalbumin-expressing interneurons coordinate hippocampal network dynamics required for memory consolidation. *Nature Communications* **8**, 15039 (2017).
18. J. Durkin *et al.*, Cortically coordinated NREM thalamocortical oscillations play an essential, instructive role in visual system plasticity. *Proceedings National Academy of Sciences* **114**, 10485-10490 (2017).
19. B. C. Clawson *et al.*, Sleep Promotes, and Sleep Loss Inhibits, Selective Changes in Firing Rate, Response Properties and Functional Connectivity of Primary Visual Cortex Neurons. *Frontiers in Systems Neuroscience* **12**, 40 (2018).
20. J. Durkin, S. J. Aton, Sleep-Dependent Potentiation in the Visual System Is at Odds with the Synaptic Homeostasis Hypothesis. *Sleep* **39**, 155-159 (2016).
21. B. C. Clawson *et al.*, Causal role for sleep-dependent reactivation of learning-activated sensory ensembles for fear memory consolidation. *Nat Communications* **12** (2021).

22. R. Boyce, S. D. Glasgow, S. Williams, A. Adamantidis, Causal evidence for the role of REM sleep theta rhythm in contextual memory consolidation. *Science* **352**, 812-816 (2016).
23. D. Miyamoto *et al.*, Top-down cortical input during NREM sleep consolidates perceptual memory. *Science* **352**, 1315-1318 (2016).
24. B. Giri, K. Diba, H. Miyawaki, S. Cheng, K. Mizuseki, Hippocampal reactivation extends for several hours following novel experience. *J Neurosci* **39**, 866-875 (2018).
25. M. Aime *et al.*, Paradoxical somatodendritic decoupling supports cortical plasticity during REM sleep. *Science* **376**, 724-730 (2022).
26. C. J. Watson, H. A. Baghdoyan, R. Lydic, Neuropharmacology of Sleep and Wakefulness. *Sleep Med Clin* **5**, 513-528 (2010).
27. F. Marrosu *et al.*, Microdialysis measurement of cortical and hippocampal acetylcholine release during sleep-wake cycle in freely moving cats. *Brain Res* **671**, 329-332 (1995).
28. V. Parikh, M. Sarter, Cholinergic mediation of attention: contributions of phasic and tonic increases in prefrontal cholinergic activity. *Ann N Y Acad Sci* **1129**, 225-235 (2008).
29. C. Barry, J. G. Heys, M. E. Hasselmo, Possible role of acetylcholine in regulating spatial novelty effects on theta rhythm and grid cells. *Front Neural Circuits* **6**, 5 (2012).
30. M. E. Hasselmo, The role of acetylcholine in learning and memory. *Curr Opin Neurobiol* **16**, 710-715 (2006).
31. B. D. Drever, G. Riedel, B. Platt, The cholinergic system and hippocampal plasticity. *Behav Brain Res* **221**, 505-514 (2011).
32. X. Li, B. Yu, Q. Sun, Z. Qiu, Generation of a whole-brain atlas for the cholinergic system and mesoscopic projectome analysis of basal forebrain cholinergic neurons. *Proc Natl Acad Sci USA* **115**, 415-420 (2017).
33. P. Dutar, M. H. Bassant, M. C. Senut, Y. Lamour, The septohippocampal pathway: structure and function of a central cholinergic system. *Physiol Rev* **75**, 393-427 (1995).
34. M. Frotscher, C. Leranth, Cholinergic innervation of the rat hippocampus as revealed by choline acetyltransferase immunocytochemistry: a combined light and electron microscopic study. *J Comp Neurol* **239**, 237-246 (1985).
35. G. Buzsaki, Theta oscillations in the hippocampus. *Neuron* **33**, 325-340 (2002).
36. J. Haam, J. L. Yakel, Cholinergic modulation of the hippocampal region and memory function. *J Neurochem* **142 Suppl 2**, 111-121 (2017).
37. E. X. Albuquerque, E. F. Pereira, M. Alkondon, S. W. Rogers, Mammalian nicotinic acetylcholine receptors: from structure to function. *Physiol Rev* **89**, 73-120 (2009).
38. K. T. Dineley, A. A. Pandya, J. L. Yakel, Nicotinic ACh receptors as therapeutic targets in CNS disorders. *Trends Pharmacol Sci* **36**, 96-108 (2015).
39. S. Jones, J. L. Yakel, Functional nicotinic ACh receptors on interneurones in the rat hippocampus. *J Physiol* **504 (Pt 3)**, 603-610 (1997).
40. A. R. McQuiston, D. V. Madison, Nicotinic receptor activation excites distinct subtypes of interneurons in the rat hippocampus. *J Neurosci* **19**, 2887-2896 (1999).
41. A. D. Fryer, A. Christopoulos, N. M. Nathanson, *Muscarinic receptors*, Handbook of experimental pharmacology, (Springer, Heidelberg, 2012), pp. xiii, 499 p.
42. D. D. Flynn, G. Ferrari-DiLeo, D. C. Mash, A. I. Levey, Differential regulation of molecular subtypes of muscarinic receptors in Alzheimer's disease. *J Neurochem* **64**, 1888-1891 (1995).
43. A. I. Levey, Muscarinic acetylcholine receptor expression in memory circuits: implications for treatment of Alzheimer disease. *Proc Natl Acad Sci U S A* **93**, 13541-13546 (1996).
44. S. Dasari, A. T. Gulledge, M1 and M4 receptors modulate hippocampal pyramidal neurons. *J Neurophysiol* **105**, 779-792 (2011).

45. F. Yi *et al.*, Direct excitation of parvalbumin-positive interneurons by M1 muscarinic acetylcholine receptors: roles in cellular excitability, inhibitory transmission and cognition. *J Physiol* **592**, 3463-3494 (2014).
46. B. S. Gutkin, G. B. Ermentrout, Dynamics of membrane excitability determine interspike interval variability: a link between spike generation mechanisms and cortical spike train statistics. *Neural Comput* **10**, 1047-1065 (1998).
47. E. M. Izhikevich, *Dynamical systems in neuroscience : the geometry of excitability and bursting*, Computational neuroscience (MIT Press, Cambridge, Mass., 2007), pp. xvi, 441 p.
48. S. A. Prescott, S. Ratte, Y. De Koninck, T. J. Sejnowski, Pyramidal neurons switch from integrators in vitro to resonators under in vivo-like conditions. *J Neurophysiol* **100**, 3030-3042 (2008).
49. C. Börgers (2017) An Introduction to Modeling Neuronal Dynamics. in *Texts in Applied Mathematics,* (Springer International Publishing : Imprint: Springer,, Cham), pp 1 online resource (XIII, 457 pages 356 illustrations, 186 illustrations in color.
50. B. Gutkin, D. Pinto, B. Ermentrout, Mathematical neuroscience: from neurons to circuits to systems. *J Physiol Paris* **97**, 209-219 (2003).
51. L. A. Bell, K. A. Bell, A. R. McQuiston, Synaptic muscarinic response types in hippocampal CA1 interneurons depend on different levels of presynaptic activity and different muscarinic receptor subtypes. *Neuropharmacology* **73**, 160-173 (2013).
52. F. Raven, S. J. Aton, The Engram's Dark Horse: How Interneurons Regulate State-Dependent Memory Processing and Plasticity. *Front Neural Circuits* **15**, 750541 (2021).
53. S. A. Raza *et al.*, HIPP neurons in the dentate gyrus mediate the cholinergic modulation of background context memory salience. *Nat Commun* **8**, 189 (2017).
54. M. Lovett-Barron *et al.*, Dendritic inhibition in the hippocampus supports fear learning. *Science* **343**, 857-863 (2014).
55. H. Nichol, B. Amilhon, F. Manseau, S. Badrinarayanan, S. Williams, Electrophysiological and Morphological Characterization of Chrna2 Cells in the Subiculum and CA1 of the Hippocampus: An Optogenetic Investigation. *Front Cell Neurosci* **12**, 32 (2018).
56. J. Delorme *et al.*, Sleep loss drives acetylcholine- and somatostatin interneuron-mediated gating of hippocampal activity to inhibit memory consolidation. *Proc Natl Acad Sci U S A* **118** (2021).
57. S. Gais, J. Born, Low acetylcholine during slow-wave sleep is critical for declarative memory consolidation. *PNAS* **101**, 2140-2144 (2004).
58. B. H. Rasch, J. Born, S. Gais, Combined blockade of cholinergic receptors shifts the brain from stimulus encoding to memory consolidation. *Journal of Cognitive Neuroscience* **18**, 793-802 (2006).
59. S. Datta, V. Mavanji, J. Ulloor, E. H. Patterson, Activation of phasic pontine-wave generator prevents rapid eye movement sleep deprivation-induced learning impairment in the rat: A mechanism for sleep-dependent plasticity. *J.Neurosci.* **24**, 1416-1427 (2004).
60. S. Datta, M. W. O'Malley, Fear extinction memory consolidation requires potentiation of pontine-wave activity during REM sleep. *J Neurosci* **33**, 4561-4569 (2013).
61. J. D. Martinez, W. P. Brancaleone, K. G. Peterson, L. G. Wilson, S. J. Aton, Atypical hypnotic compound ML297 restores sleep architecture immediately following emotionally valenced learning, to promote memory consolidation and hippocampal network activation during recall *Sleep* **46**, zsac301 (2023).
62. E. A. McDevitt, K. A. Duggan, S. C. Mednick, **REM sleep rescues learning from interference.**

. *Neurobiol Learn Mem* **122**, 51-62 (2015).
63. A. D. Grosmark, G. Buzsaki, Diversity in neural firing dynamics supports both rigid and learned hippocampal sequences. *Science* **351**, 1440-1443 (2016).

64. J. P. Roach, B. Eniwaye, V. Booth, L. M. Sander, M. R. Zochowski, Acetylcholine Mediates Dynamic Switching Between Information Coding Schemes in Neuronal Networks. *Front Syst Neurosci* **13**, 64 (2019).
65. K. M. Stiefel, B. S. Gutkin, T. J. Sejnowski, The effects of cholinergic neuromodulation on neuronal phase-response curves of modeled cortical neurons. *Journal of Computational Neuroscience* **26**, 12 (2009).
66. B. S. Gutkin, G. B. Ermentrout, A. D. Reyes, Phase-response curves give the responses of neurons to transient inputs. *J Neurophysiol* **94**, 1623-1635 (2005).
67. R. M. Smeal, G. B. Ermentrout, J. A. White, Phase-response curves and synchronized neural networks. *Philos Trans R Soc Lond B Biol Sci* **365**, 2407-2422 (2010).
68. C. Borgers, S. Epstein, N. J. Kopell, Background gamma rhythmicity and attention in cortical local circuits: a computational study. *Proc Natl Acad Sci U S A* **102**, 7002-7007 (2005).
69. M. A. Whittington, R. D. Traub, N. Kopell, B. Ermentrout, E. H. Buhl, Inhibition-based rhythms: experimental and mathematical observations on network dynamics. *Int J Psychophysiol* **38**, 315-336 (2000).
70. J. Born, B. Rasch, S. Gais, Sleep to remember. *Neuroscientist* **12**, 410-424 (2006).
71. G. Tononi, C. Cirelli, Sleep function and synaptic homeostasis. *Sleep Med Rev* **10**, 49-62 (2006).
72. A. D. Grosmark, K. Mizuseki, E. Pastalkova, K. Diba, G. Buzsaki, REM sleep reorganizes hippocampal excitability. *Neuron* **75**, 1001-1007 (2012).
73. S. McKenzie, Inhibition shapes the organization of hippocampal representations. *Hippocampus* **28**, 659-671 (2018).
74. J. Csicsvari, H. Hirase, A. Czurko, A. Mamiya, G. Buzsaki, Oscillatory coupling of hippocampal pyramidal cells and interneurons in the behaving Rat. *J Neurosci* **19**, 274-287 (1999).
75. L. Marshall *et al.*, Hippocampal pyramidal cell-interneuron spike transmission is frequency dependent and responsible for place modulation of interneuron discharge. *J Neurosci* **22**, RC197 (2002).
76. E. Stark, L. Roux, R. Eichler, G. Buzsaki, Local generation of multineuronal spike sequences in the hippocampal CA1 region. *Proc Natl Acad Sci U S A* **112**, 10521-10526 (2015).
77. F. Wu *et al.*, Monolithically Integrated muLEDs on Silicon Neural Probes for High-Resolution Optogenetic Studies in Behaving Animals. *Neuron* **88**, 1136-1148 (2015).
78. K. K. Tayler, K. Z. Tanaka, L. G. Reijmers, B. J. Wiltgen, Reactivation of neural ensembles during the retrieval of recent and remote memory. *Curr Biol* **23**, 99-106 (2013).
79. T. Stefanelli, C. Bertollini, C. Luscher, D. Muller, P. Mendez, Hippocampal Somatostatin Interneurons Control the Size of Neuronal Memory Ensembles. *Neuron* **89**, 1074-1085 (2016).
80. H. C. Barron, Neural inhibition for continual learning and memory. *Curr Opin Neurobiol* **67**, 85-94 (2021).
81. B. Rudy, G. Fishell, S. Lee, J. Hjerling-Leffler, Three groups of interneurons account for nearly 100% of neocortical GABAergic neurons. *Dev Neurobiol* **71**, 45-61 (2011).
82. M. J. Bezaire, I. Soltesz, Quantitative assessment of CA1 local circuits: knowledge base for interneuron-pyramidal cell connectivity. *Hippocampus* **23**, 751-785 (2013).
83. E. Stark *et al.*, Pyramidal cell-interneuron interactions underlie hippocampal ripple oscillations. *Neuron* **83**, 467-480 (2014).
84. C. Morales *et al.*, Dentate Gyrus Somatostatin Cells are Required for Contextual Discrimination During Episodic Memory Encoding. *Cereb Cortex* **31**, 1046-1059 (2021).
85. Y. Jia, Y. Yamazaki, S. Nakauchi, K. Ito, K. Sumikawa, Nicotine facilitates long-term potentiation induction in oriens-lacunosum moleculare cells via Ca2+ entry through non-alpha7 nicotinic acetylcholine receptors. *Eur J Neurosci* **31**, 463-476 (2010).

86. H. Kametani, H. Kawamura, Alterations in acetylcholine release in the rat hippocampus during sleep-wakefulness detected by intracerebral dialysis. *Life Sci* **47**, 421-426 (1990).
87. L. M. Teles-Grilo Ruivo *et al.*, Coordinated Acetylcholine Release in Prefrontal Cortex and Hippocampus Is Associated with Arousal and Reward on Distinct Timescales. *Cell Rep* **18**, 905-917 (2017).
88. G. P. Krishnan *et al.*, Cellular and neurochemical basis of sleep stages in the thalamocortical network. *Elife* **5** (2016).
89. A. Eban-Rothschild, L. Appelbaum, L. de Lecea, Neuronal Mechanisms for Sleep/Wake Regulation and Modulatory Drive. *Neuropsychopharmacology* **43**, 937-952 (2018).
90. I. B. Iotchev, E. Kubinyi, Shared and unique features of mammalian sleep spindles - insights from new and old animal models. *Biol Rev Camb Philos Soc* **96**, 1021-1034 (2021).
91. C. G. Fink, G. G. Murphy, M. Zochowski, V. Booth, A dynamical role for acetylcholine in synaptic renormalization. *PLOS Computational Biology* **9** (2013).
92. J. Wu *et al.*, Functional network stability and average minimal distance – A framework to rapidly assess dynamics of functional network representations. *Journal of Neuroscience Methods* **296**, 15 (2018).